

## Article

# Solid-State Lithium Batteries with Cathode-Supported Composite Solid Electrolytes Enabling High-Rate Capability and Excellent Cyclic Performance

Kang-Feng Chang <sup>1</sup>, Pradeep Kumar Panda <sup>1</sup>, Chien-Te Hsieh <sup>1,2,\*</sup>, Po-Chih Yang <sup>1,\*</sup>, Navish Kataria <sup>3</sup> and Kuan Shiong Khoo <sup>1,4,\*</sup>

<sup>1</sup> Department of Chemical Engineering and Materials Science, Yuan Ze University, Taoyuan 32003, Taiwan; ct523999@gmail.com (K.-F.C.); rkpanda277@gmail.com (P.K.P.)

<sup>2</sup> Department of Mechanical, Aerospace, and Biomedical Engineering, University of Tennessee, Knoxville, TN 37996, USA

<sup>3</sup> Department of Environmental Sciences, J.C. Bose University of Science and Technology, YMCA, Faridabad 121006, Haryana, India; navishkataria08@gmail.com

<sup>4</sup> Centre for Herbal Pharmacology and Environmental Sustainability, Chettinad Hospital and Research Institute, Chettinad Academy of Research and Education, Kelambakkam, Chennai 603103, Tamil Nadu, India

\* Correspondence: cthsieh@saturn.yzu.edu.tw (C.-T.H.); pcyang@saturn.yzu.edu.tw (P.-C.Y.); kuanshiong.khoo@saturn.yzu.edu.tw (K.S.K.)

**Abstract:** In this study, robust composite solid electrolytes were developed and employed to enhance the performance of Li-metal batteries significantly. The robust composite solid electrolytes are composed of a soft polymer, poly(ethylene oxide), a Li salt, bis(trifluoromethanesulfonyl)imide (LiTFSI), and super ionic conductive ceramic fillers such as  $\text{Li}_{1.5}\text{Al}_{0.5}\text{Ti}_{1.5}(\text{PO}_4)_3$  (LATP), and  $\text{Li}_{6.4}\text{La}_3\text{Zr}_{1.4}\text{Ta}_{0.6}\text{O}_{12}$  (LLZTO). The main goal of this study is to enhance the electrochemical stability and ionic conductivity. The ionic conductivities of the composite solid electrolytes were found to be  $2.08 \times 10^{-4}$  and  $1.64 \times 10^{-4} \text{ S cm}^{-1}$  with the introduction of LATP and LLZTO fillers, respectively. The results prove that the fabricated solid electrolyte was electrochemical stable at voltage exceeding 4.25 V vs. Li/Li<sup>+</sup>. The internal resistance of the solid electrolyte significantly reduced compared to gel electrolyte. This reduction can be attributed to the alleviation of bulk electrolyte, charge-transfer, and interfacial electrolyte/electrode impedance. When LiFePO<sub>4</sub> cathode sheets are coated with a composite solid electrolyte containing LATP powders, the resulting Li-metal battery displays high capacity at 5 C (with a capacity retention of 65.2% compared to the original capacity at 0.2 C) as well as superior cyclic stability and excellent Coulombic efficiency (>99.5%, 200 cycles). These results confirm that the composite solid electrolyte acts as a protective layer which has the ability to prevent the growth of Li dendrites. Consequently, the fabricated electrolyte configuration can be engineered to enable high energy/power density and electrochemical stable cyclability in Li-metal batteries.



**Citation:** Chang, K.-F.; Panda, P.K.; Hsieh, C.-T.; Yang, P.-C.; Kataria, N.; Khoo, K.S. Solid-State Lithium Batteries with Cathode-Supported Composite Solid Electrolytes Enabling High-Rate Capability and Excellent Cyclic Performance. *Batteries* **2023**, *9*, 490. <https://doi.org/10.3390/batteries9100490>

Received: 26 August 2023

Revised: 18 September 2023

Accepted: 23 September 2023

Published: 26 September 2023



**Copyright:** © 2023 by the authors. Licensee MDPI, Basel, Switzerland. This article is an open access article distributed under the terms and conditions of the Creative Commons Attribution (CC BY) license (<https://creativecommons.org/licenses/by/4.0/>).

## 1. Introduction

Liquid organic electrolyte (LOE)-based lithium-ion batteries (LIBs) have gained a lot of attention for many years and utilize a variety of applications owing to their outstanding combination of high-power density and energy. They are ideal for use in electric vehicles, portable electronic devices, and other industries [1,2]. However, LOE is a volatile and flammable electrolyte, which elevates major problems for LIBs development. The risk of thermal runaway and potential explosion or catastrophic fires associated with these electrolytes has severely impacted their progress [3,4]. Thus, solid-state LIBs are regarded as the most promising next-generation lithium batteries. Solid-state electrolytes are preferred over liquid electrolytes because they eliminate safety concerns and allow for higher energy

density by using high-capacity electrodes like high-voltage cathodes, Li metal anodes, and conversion-type sulfur and oxygen electrodes [5–8]. Usually in solid state batteries, a separator was introduced to avoid direct contact between two electrodes, while enabling ion flow between them. The ion movements are crucial for battery performance as it produces electrical energy, but solid-state electrolytes act as both separator and electrolyte. Like liquid electrolyte, separator can conduct ions as well as separate the electrolytes, which simplifies the battery fabrication process. Additionally, separator can provide battery safety, stability, and credibility. Moreover, solid state electrolyte has no chance of leakage and short circuit during its uses, unlike liquid electrolyte [9]. Therefore, solid state electrolyte is a safer option to use in batteries as electrolyte. Overall, the use of solid-state electrolytes as both an electrolyte and a separator simplify the battery fabrication process, while improving its safety and reliability. This is an important development in the field of battery technology, as it can help to reduce the cost and complexity of manufacturing batteries while also improving their performance and safety.

Solid-state batteries must have solid-state electrolytes to achieve high electrochemical and mechanical stability. This electrolyte not only enhances the performance of the batteries but also provides a high compatible interface between two electrodes. Therefore, selecting the appropriate type of solid electrolyte and developing the right composition are critical factors for the battery's performance. The most essential component i.e., solid state electrolyte, can be broadly categorized into two types such as solid polymer electrolytes and inorganic (i.e., ceramics) electrolytes [3,10,11]. There are numerous studies of solid inorganic electrolyte such as  $\text{Li}_{1.5}\text{Al}_{0.5}\text{Ti}_{1.5}(\text{PO}_4)_3$  (LATP) and  $\text{Li}_{6.4}\text{La}_3\text{Zr}_{1.4}\text{Ta}_{0.6}\text{O}_{12}$  (LLZTO) owing to their wide electrochemical window, high conductivity i.e.,  $\sim 10^{-4} \text{ S cm}^{-1}$  at ambient temperature, and strong electrochemical stability [12,13]. However, its practical applications are hindered due to great interfacial resistance between brittle ceramic electrodes and electrolytes [14–16]. In contrast, polymer-based composite solid electrolytes which incorporate Li salts and diverse functional fillers have garnered significant interest due to their favorable attributes for commercial applications. These include their ease of processing and flexibility [17–20]. However, poly(ethylene oxide) (PEO)-based composite solid electrolytes possessed low ionic conductivity ( $< 10^{-5} \text{ S cm}^{-1}$ ) and a narrow electrochemical window ( $< 3.9 \text{ V}$ ) at ambient temperature, which hindered its practical uses [13,14]. Based on the above deduction, one strategy is to offer a synergistic effect on the novel design of “ceramic-in-polymer” or “polymer-in-ceramic” electrolytes that combines highly ionic conductive ceramics (e.g., LATP and LLZTO) and highly flexible and processible polymers (e.g., PEO), capable of offering a feasibility for high-performance solid-state Li-metal batteries [21,22]. Such a design can provide a feasible approach for developing high-performance solid-state Li-metal batteries. To enhance the electrochemical performance of solid-state batteries, the development of solid composite electrolytes (i.e., “ceramic-in-polymer” or “polymer-in-ceramic” electrolytes) has been explored, such as PEO + LLZTO [23] and poly(vinylidene fluoride-co-hexafluoropropene) + LATP [11,24]. However, even though ionic conductivity has improved significantly in recent years, Li dendrites and the possibility of penetration through “ceramic-in-polymer” electrolytes can lead to short circuits in solid-state batteries, severely limiting their practical use.

The development of composite solid electrolytes has shown promise in enhancing the cyclic stability of solid-state batteries, which is important in the context of the issues experienced by solid-state batteries. However, issues such as Li dendrite formation and short circuits still hinder their practical applications. This study aims to address these issues and unlock the full potential of solid-state batteries as a reliable and sustainable energy storage solution. To achieve this goal, this work proposes depositing “ceramic-in-polymer” electrolytes on the cathode side to create conductive and stable interfaces, minimizing interfacial resistance and mechanical stress during extended cycling. Two types of composite solid electrolytes, PEO + LLZTO + LiTFSI and PEO + LATP + LiTFSI, are coated on the  $\text{LiFePO}_4$  (LFP) cathode to create high-performance Li-metal batteries. This research aids in the design of high-performance solid-state batteries by providing insight

into the applicability of composite solid electrolytes for usage on both the LFP cathode and Li anode side. High energy/power density and stable cyclability could be achieved with these composite solid electrolytes because of their high compatibility with the cathode and anode and their ability to inhibit Li dendrite growth.

## 2. Experimental Section

### 2.1. Fabrication of Composite Solid Electrolytes

In this work, poly(ethylene oxide) (PEO, formula:  $(-\text{CH}_2\text{CH}_2\text{O}-)_n$ , molar mass =  $3 \times 105 \text{ g mol}^{-1}$ , melting point: 65 °C, Aladdin City, FL, USA) and lithium bis(trifluoromethanesulfonyl)imide (LiTFSI, formula:  $\text{LiC}_2\text{NO}_4\text{F}_6\text{S}_2$ , molar mass: 287.1 g mol $^{-1}$ , Sigma-Aldrich, St. Louis, MO, USA, 99.95%) were dried at 80 °C for 12 h under vacuum prior the fabrication of composite solid electrolytes. 1-methyl-2-pyrrolidone (NMP, Sinopharm, Hong Kong) and acetonitrile (ACN, Aladdin, USA) were used as received.

Two types of composite gel electrolytes were prepared using different ratios of PEO and LiTFSI in weight/weight (*w/w*). The first ratio was 2/1 (PEO/LiTFSI), and the second ratio was 3/1 (PEO/LiTFSI). The gel electrolytes were prepared by dissolving the PEO/LiTFSI mixtures (3.678 gm) in 15 mL of ACN under continuous stirring at 30 °C for 6 h. The resulting slurries were used for fabricating gel electrolytes supported by LFP cathode sheets. The samples with the PEO/LiTFSI ratio of 2/1 and 3/1 were denoted as PL21 and PL31, respectively. Subsequently, the PL slurries were mixed with 20 wt% ceramic powders, namely, lithium aluminum titanium phosphate (LATP) and lithium lanthanum zirconium tantalum oxide (LLZTO), with stirring at 50 °C for 6 h to achieve a homogeneous electrolyte slurry. The samples mixed with LATP and LLZTO powders were labeled as PL31-LATP and PL31-LLZTO, respectively. Both slurries were then used for fabricating composite solid electrolytes supported by LFP cathode.

### 2.2. Fabrication of LFP-Supported Composite Solid Electrolytes

In order to produce the LFP cathode, olivine-type LFP powders (particle size around 500 nm) were combined with a polyvinylidene fluoride binder (PVDF), and a conducting medium (Super-P, Taiwan Maxwave Co., Taiwan) in NMP solvent (40 mL). The ratio of the above components was 90:7:3 (*w/w/w*), respectively, resulting in the formation of an LFP slurry. Then the slurry was mixed for 2 h using a 3D mixer (SPEX-8000D, Qingdao, China) with Zr balls to ensure uniformity. The aforementioned slurry was applied to Al foil using a doctor blade. The above produced LFP cathode sheets were dried overnight in a vacuum oven at 110 °C, compacted, and then cut into the proper form for battery assembly. The fabrication process for LFP-supported composite solid electrolytes involved four configurations (PL21, PL31, PL31-LATP, and PL31-LLZTO). The electrolyte slurries were deposited onto the LFP cathode, and the thickness (60 µm) of each composite layer was precisely controlled using a doctor blade. To maintain good adhesion, all samples were kept in a vacuum oven at 140 °C for overnight.

### 2.3. Materials and Electrochemical Characterization

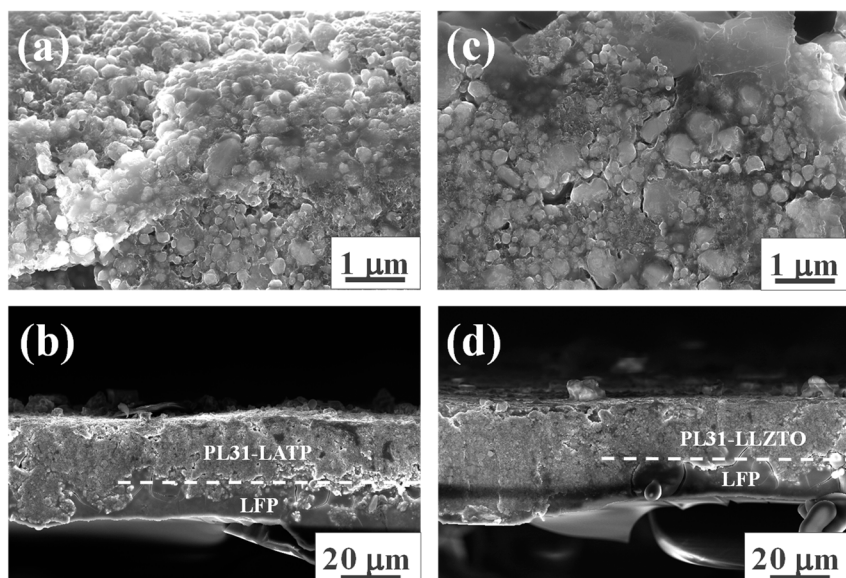
The morphology of the LFP-supported composite solid electrolytes was investigated through field-emission scanning electron microscopy (FE-SEM, JEOL JSM-6700F). The X-ray diffraction (XRD) patterns of composite solid electrolytes were obtained using diffractometer (Bruker D2, Karlsruhe, Germany) equipped with a copper (Cu) target. To determine the maximum potential of each composite solid electrolyte in symmetric cells with Li metal, linear scanning voltammetry was employed. Electrochemical impedance spectroscopy (EIS) was used to evaluate the polarization of coin cells constructed with different LFP-supported composite electrolytes in the 100 kHz to 10 mHz frequency range. EIS measurements were done by utilizing a CH Instruments 608C instrument (Anatech Co. Ltd., Taiwan).

For electrochemical performance measurements of the LFP-supported composite solid electrolytes, coin cells (CR2032 type) were utilized. The fabricated LFP-supported composite electrolytes were inserted into the coin-cell kits, and Li-metal batteries were

assembled within a glove box (MBARUN, China). The charge/discharge cycle tests used to evaluate the real-time performance of the LFP-supported composite electrolytes ranged from 0.2 to 5 C within the voltage range of 2.4–4.0 V at room temperature. The cyclic performance of Li-metal batteries was tested for 200 cycles at 0.2 C (charging) and 0.5 C (discharging).

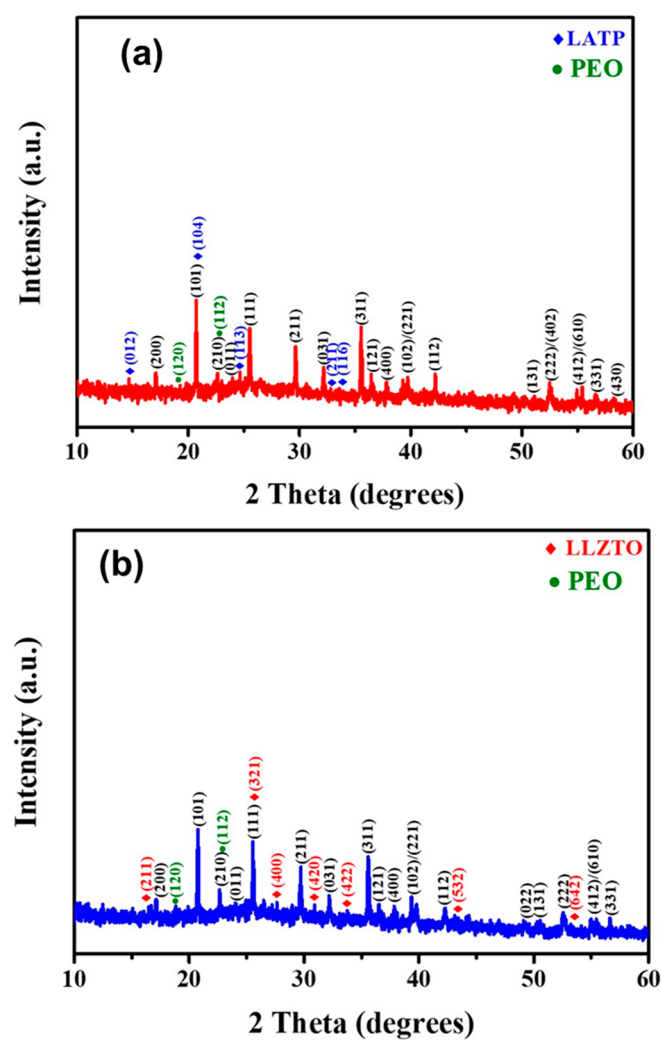
### 3. Results and Discussion

Figure 1 displays the FESEM images (Top- and cross-sectional) of the PL31-LATP and PL31-LLZTO electrolytes. The top-view images reveal a roughened surface consisting of numerous ceramic particles embedded in flexible PEO polymer. The cross-sectional views demonstrate that the composite solid electrolytes are tightly attached to the LFP cathode sheets, with a thickness of approximately 25–30  $\mu\text{m}$  for both solid electrolytes. There is no visible distinction observed at the interface between the composite solid electrolytes and the LFP cathode sheets, which are covered by a smooth coating of composite solid electrolytes. These findings led to the conclusion that the “ceramic-in-polymer” electrolytes are very cohesive and highly flexible.



**Figure 1.** Top and cross-sectional views of FE-SEM images: (a,b) PL31-LATP and (c,d) PL31-LLZTO sample on LFP cathode sheets.

The XRD patterns of PL31-LATP and PL31-LLZTO samples on LFP cathode sheets are displayed in Figure 2. The LFP sample exhibited various diffraction peaks which are well matched with the standard orthorhombic olivine phase of LFP (JCPDS Card No.: 83-2092:  $a = 10.334 \text{ \AA}$ ,  $b = 6.010 \text{ \AA}$ , and  $c = 4.693 \text{ \AA}$ ) [25], confirming the highly crystalline nature of the LFP powders [26]. The XRD patterns also show two diffraction peaks at 19.2 and 23.6°, which can be assigned to the (120) and (112) crystalline planes of PEO crystals, respectively [27]. The weak diffraction peaks are attributed to the ceramics (i.e., LATP and LLZTO) inserted into the PEO network, which reduces the crystalline degree of PEO polymers [28]. The XRD pattern of LATP powder for the PL31-LATP sample matches the typical NASICON-type structure with rhombohedral lattice (Card No.: ICDD 00-035-0754). The XRD peaks are positioned at 24.5, 29.7, and 36.5°, which correspond to (104), (113), and (116), respectively [29,30]. However, the PL31-LLZTO sample’s diffraction peaks closely correspond to the typical pattern of cubic-LLZTO (ICSD Card No.: 45-109), confirming the existence of a cubic phase LLZTO [31,32]. Overall, the XRD patterns of both PL31-LATP and PL31-LLZTO samples confirm the solid composite nature of the materials, consisting of olivine-type LFP, amorphous PEO, and crystalline ceramics (LATP and LLZTO crystals) without any impurity.



**Figure 2.** Typical XRD patterns of (a) PL31-LATP and (b) PL31-LLZTO sample on LFP cathode sheets.

LSV is an important technique used to study the electrochemical behavior materials by sweeping the potential applied to an electrode or electrolyte at a constant rate. In the context of characterizing composite solid electrolytes, LSV was employed to determine the breakdown potential of each electrolyte sample. This was done by subjecting the electrolyte at a scan rate of  $0.1 \text{ mV s}^{-1}$ , as illustrated in Figure 3a. The following experiment's LSV profiles demonstrated composite electrolytes' electrochemical stability. The results revealed that composite electrolytes possessed high breakdown potentials exceeding 4.25 V compared to the Li/Li<sup>+</sup> reference electrode. This finding is crucial because it indicates that these solid electrolytes can withstand high potentials without undergoing significant degradation or decomposition. The tendency of solid electrolytes to maintain stability at high potentials implies that they may efficiently assist the operation of high-voltage cathodes, allowing the development of new energy storage systems with enhanced performance and energy density. Figure 3b,c demonstrates the Nyquist plots of LFP-supported composite electrolytes before and after cycling test (50 cycles), respectively. Over the frequency range, Nyquist plots show one charge-transfer impedance depressed semicircle comprising the electrode/electrolyte contact across the frequency range [33]. Accordingly, one equivalent circuit model (see Figure 3d) can be proposed with the combination of components including R1 (the resistance of bulk electrolyte), R2 (the interfacial impedance of the electrolyte/electrode interface, i.e., the resistance of solid electrolyte interphase (SEI) layer)), R3 (the interfacial impedance of charge transfer resistance), and CPE (the constant phase elements for double layer capacitance) [34]. Z-view software was used to investigate the

EIS spectra of LFP-supported composite solid electrolytes. The experimental impedance spectra and model predictions were within 10% throughout the frequency range. The equivalent series resistance ( $ESR = R_1 + R_2 + R_3$ ) could be calculated from Figure 4a to estimate the cells' total internal resistance [35]. Before cycling, the ESR values of PL21, PL31, PL31-LATP, and PL31-LLZTO samples are found to be 726, 536, 141, and 162  $\Omega$ , respectively. After cycling, the ESR values are decreased to 199, 192, 87, and 113  $\Omega$  for PL21, PL31, PL31-LATP, and PL31-LLZTO samples, respectively. The reduced magnitude in ESR measurements when compared to before cycling may be ascribed to the formation of an ionically conductive electrolyte. This result reveals that the ESR value (i.e., the overall inner resistance) is significantly decreased by the robust design of composite solid electrolytes (i.e., PL31-LATP and PL31-LLZTO) as compared to gel electrolyte, attributed to the fact that the bulk electrolyte, interfacial electrolyte/electrode impedance, and charge-transfer is substantially alleviated. Overall, the analysis of Nyquist plots and ESR values provides valuable information regarding the internal resistance and electrochemical behavior of composite solid electrolytes, which is critical for designing high-performance energy storage devices. Further, ionic conductivity ( $\sigma$ ) was evaluated using EIS plots using this formula  $\sigma = l/(R_1 \times A)$ , where ' $l$ ' is the thickness of the film in the electrolyte, and ' $A$ ' is the projected active area [27,36]. The  $\sigma$  values follows the following order: PL31-LATP ( $2.08 \times 10^{-4} \text{ S cm}^{-1}$ ) > PL31-LLZTO ( $1.64 \times 10^{-4} \text{ S cm}^{-1}$ ) > PL31 ( $8.58 \times 10^{-5} \text{ S cm}^{-1}$ ) > PL21 ( $5.10 \times 10^{-5} \text{ S cm}^{-1}$ ) and are presented in Figure 4b. Further, we compared our ionic conductivity results with previous studies and provided a comparative table in supplementary information (Table S1). The PL31-LATP and PL31-LLZTO samples have better ionic conductivities than the PL21 and PL31 samples owing to the formation of a dense layered structure (Figure 1b,d). PEO polymer matrixes and ceramic particles construct this layer structure [37,38]. Solid electrolytes for Li-metal batteries provide the aforesaid high ionic conductivity. The crystalline degree of PEO polymers reduced due to the introduction of moderate amounts of LATP and LLZTO fillers. The ionic segmental motion is enhanced due to the reduction of crystalline in composite electrolytes. This enhanced segmental motion promotes ion mobility inside the composite electrolyte, resulting in greater ionic conductivity. Moreover, percolation behavior phenomenon was observed at the interface between LATP/LLZTO particles and PEO polymer matrix [39,40]. This percolation behavior further enhances the movement of  $\text{Li}^+$  ions, facilitating faster ionic conduction and contributing to enhanced ionic conductivity [23,41]. Accordingly, the quantification of ionic conductivity using EIS analysis reveals that the design of composite solid electrolytes, particularly those incorporating LATP and LLZTO fillers, significantly enhances the ionic conductivity in Li-metal batteries. The 3D ionic conductive network formed within the composite electrolyte, along with the reduced crystalline degree of the polymer and percolation behavior at the interface, collectively contribute to the improved ionic conductivity and have the potential for developing high-performance energy storage technology.

To evaluate the high-rate capability, galvanostatic charge-discharge profiles of solid electrolytes were recorded, which is equipped with Li-metal batteries and presented in Figure 5a–d. The Li-metal batteries were cycled through voltages of 2.4 to 4.0 V (vs.  $\text{Li}/\text{Li}^+$ ) at charge and discharge rates of 0.2, 0.5, 1, 2, and 5 C. At 0.2 C, all batteries showed a distinct flat plateau, suggesting a two-phase reversible process:  $\text{LiFePO}_4 \leftrightarrow (1-x)\text{LiFePO}_4 + x\text{FePO}_4 + x\text{Li}^+ + xe^-$ . The estimated specific capacity for this reaction is around  $170 \text{ mAh g}^{-1}$ , measured at Ca. 3.2 – 3.6 V vs.  $\text{Li}/\text{Li}^+$  [42]. All battery discharge capacities attained approximately  $160 \text{ mAh g}^{-1}$ , which is close to the estimated capacity. Furthermore, symmetry was observed in the 0.2 C charge/discharge curves, indicating Li ions in the olivine-type LFP crystals.

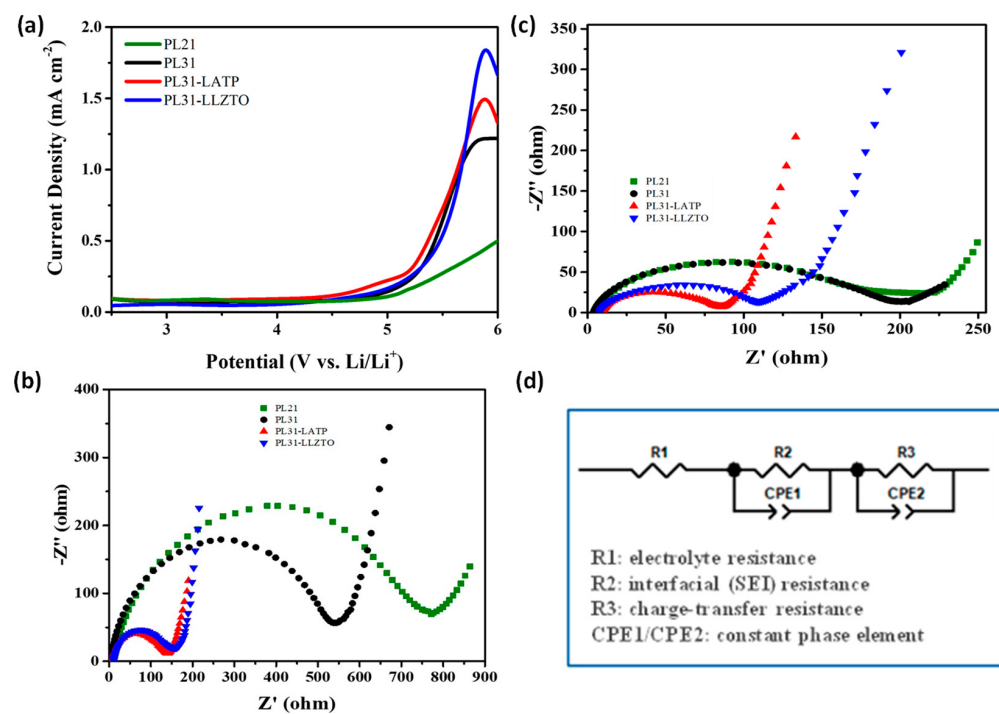


**Figure 3.** (a) LSV curves of different SSE samples, Nyquist plots of symmetric cells using different SSE samples (b) before and (c) after cycling test, and (d) the proposed equivalent circuit, consisting of electrolyte resistance, interfacial resistance, charge-transfer resistance, and two constant phase elements.

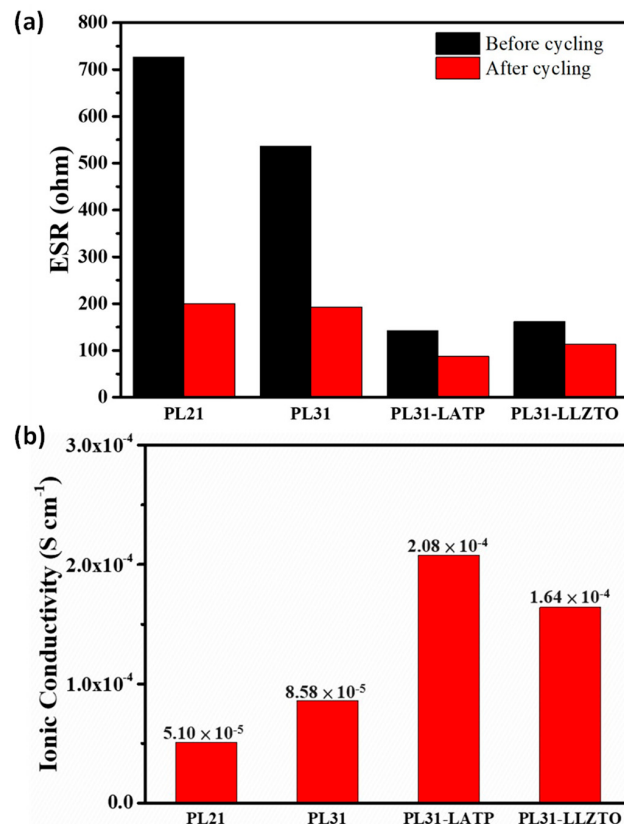


**Figure 4.** (a) ESR and (b) ionic conductivity of different SSE samples.

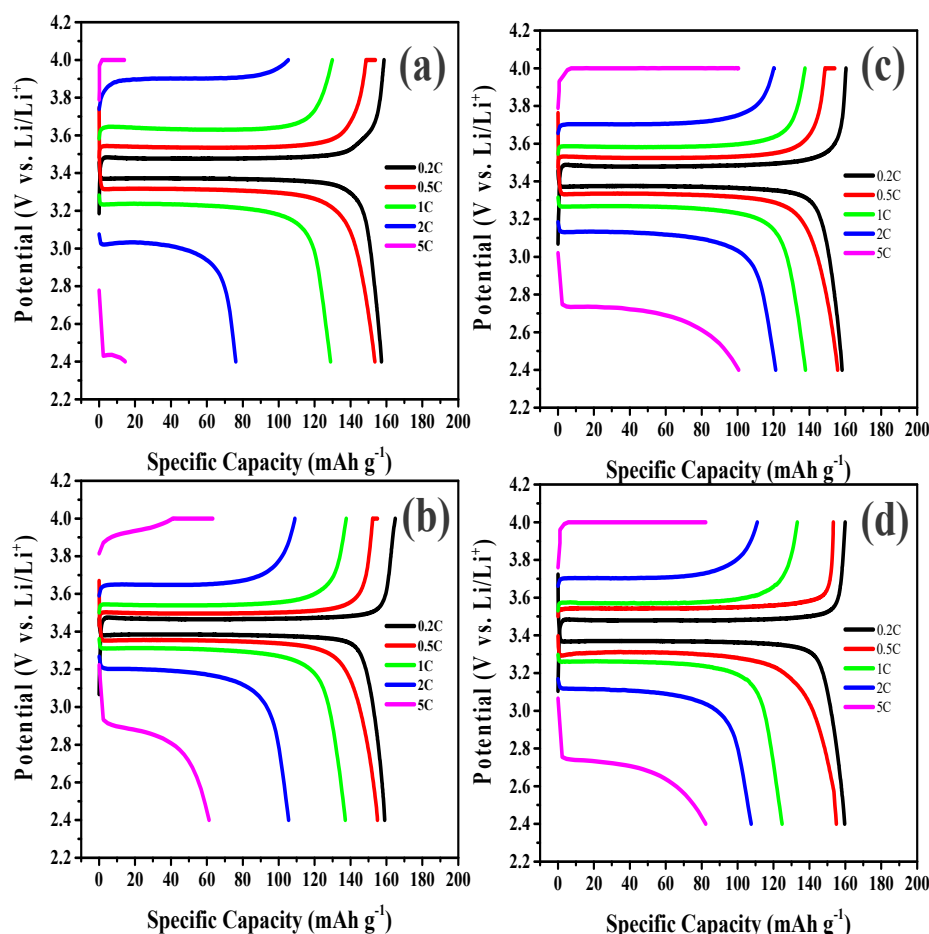


**Figure 5.** Typical charge-discharge curves of Li-metal batteries equipped with (a) PL21, (b) PL31, (c) PL31-LATP, and (d) PL31-LLZTO electrolytes at various rates.

Electrode polarization (represented by the potential difference between charging and discharging plateaus,  $\Delta E$ ) was significantly influenced by the electrolyte type, particularly at high-rate capacities such as 2 C and 5 C. With higher C rates, the  $\Delta E$  increased due to the apparent polarization resulting from ionic diffusion and charge transfer resistance in the Li-metal batteries. As shown by the discharge capacity vs C rate plot, the Li-metal battery fabricated using the PL31-LATP electrolyte displayed improved rate capability across the entire 0.2–5 C rate range (see Figure 6a). The capacity retentions were 96.2% (0.5 C), 83.9% (1 C), 75.8% (2 C), and 65.2% (5 C) compared to the discharge capacity at 0.2 C, confirming its high-rate capabilities. After the rate capability test, all Li-metal batteries recovered to their original capacity at 0.2 C, indicating excellent  $\text{Li}^+$  reversibility through the robust design of the hierarchical composite solid layer, even after high-rate cycling experiments. In contrast, both PL21 and PL31 samples displayed poor high-rate capability at 5 C, indicating significant electrode polarization. The enhanced rate capacity compared to the PL31-LATP sample underlined the relevance of LATP fillers in the construction of composite solid electrolytes.

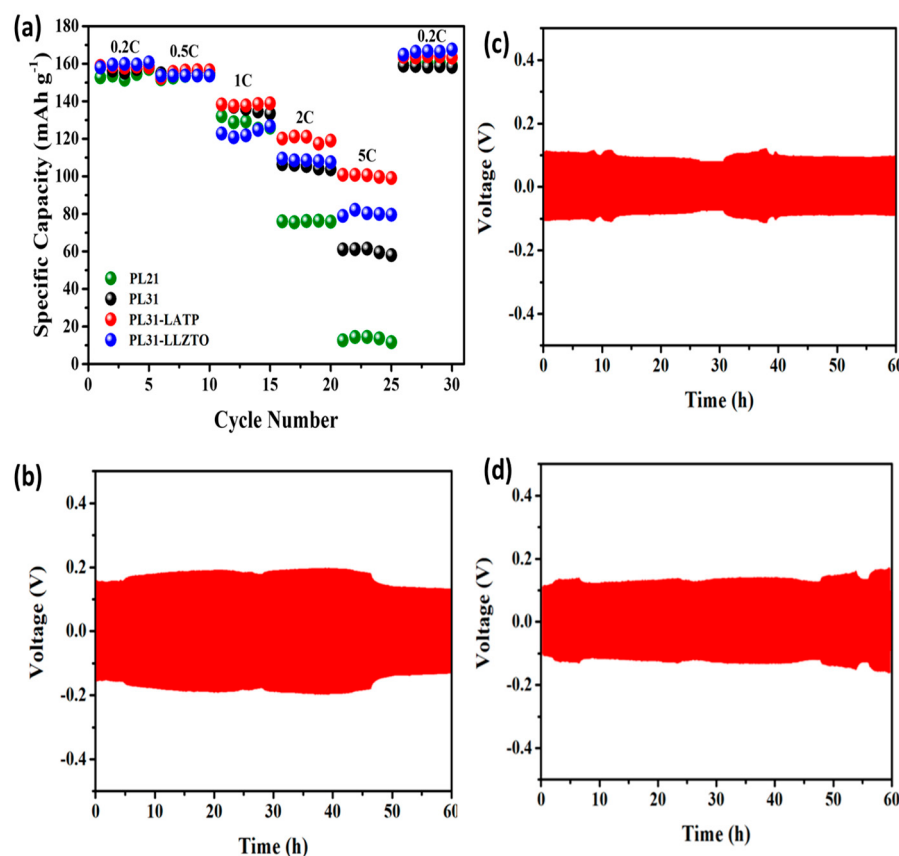


**Figure 6.** (a) Variation of discharge capacity with C rate for different Li-metal batteries, and galvanostatic cycles of Li symmetric cells using different solid electrolytes: (b) PL31, (c) PL31-LATP, and (d) PL31-LLZTP at  $0.2 \text{ mA cm}^{-2}$ .

Figure 6b–d demonstrate galvanostatic cycles of Li symmetric cells using several solid-state electrolytes (PL31, PL31-LATP, and PL31-LLZTO samples) at a current density of  $0.2 \text{ mA cm}^{-2}$  to evaluate the durability. This analysis was carried out to evaluate the electrochemical stability of the composite electrolytes in the presence of Li metal. The whole galvanostatic cycling analysis was done at ambient temperature. According to the findings, Li symmetric cells equipped with composite electrolytes that contained soft PEO electrolytes without LLZTO fillers (PL31) displayed unstable Li plating/stripping cycling for about 60 h before incurring a short circuit. Notably, the Li-dendrite-suppression capability of the composite electrolyte gradually improved with the incorporation of LATP and LLZTO fillers. Particularly noteworthy, the Li symmetric cells fabricated with PL31-LATP and PL31-LLZTO electrolytes demonstrated stable cycling without short circuits for 60 h. These results suggest the potential of these batteries for enhanced safety and improved electrochemical stability in Li metal. This enhancement is due to the high amount of LLZTO ceramic, which has a shear modulus of up to 55 GPa, significantly more than the minimal value (8.5 GPa), necessary to inhibit Li dendrite growth [43]. As per the previous finding, LATP powders modulus of elasticity and hardness values vary from 107–150 GPa to 5.5–10.0 GPa, respectively [44]. Therefore, it is necessary to introduce highly conductive ceramics as fillers into composite electrolytes in order to increase the mechanical strength, which acts as a physical barrier to suppress Li dendrites [45].

The typical charge-discharge curves of Li-metal batteries fabricated with LFP-supported solid-state electrolytes (PL31-LATP and PL31-LLZTO) are presented in Figure 7a,b. Charge/discharge analysis of the Li-metal batteries was conducted under ambient temperature with potential window 2.4–4.0 V vs.  $\text{Li}/\text{Li}^+$ . The batteries were charged at a rate of 0.2 C and discharged at a rate of 0.5 C. Significantly, both Li-metal batteries exhibit a stable

reversible capacity spanning from 153 to 160 mAh g<sup>-1</sup> in 200 cycles, which represents over 90% energy storage within the olivine LFP lattices. In addition, the charge/discharge curves exhibit symmetry at 0.2 C/0.5 C, indicating that Li<sup>+</sup> intercalation and de-intercalation are reversible. Figure 7c,d displays the capacity retention and Coulombic efficiency as a function of cycle number for both Li-metal batteries fabricated with LFP-supported solid-state electrolytes in order to evaluate their cyclic performance. Coulombic efficiency and capacity retention are commonly electrochemical parameters of an energy device, which are used to assess the cyclic stability of composite solid electrolytes during charge/discharge cycling. These parameters (Coulombic efficiency and capacity retention) are estimated as per the previous study [46]. Remarkably, in 200 cycles, both Li-metal batteries demonstrate superior cyclic performance with excellent Coulombic efficiency (>99.5%). This satisfactory result confirms that the composite solid electrolyte consisting of PEO, ceramics (LATP and LLZTO), and LiTFSI offers a protective layer against Li dendrite growth. Consequently, it induces desirable cyclic stability and superior rate capability, ensuring the long-term performance of the batteries.

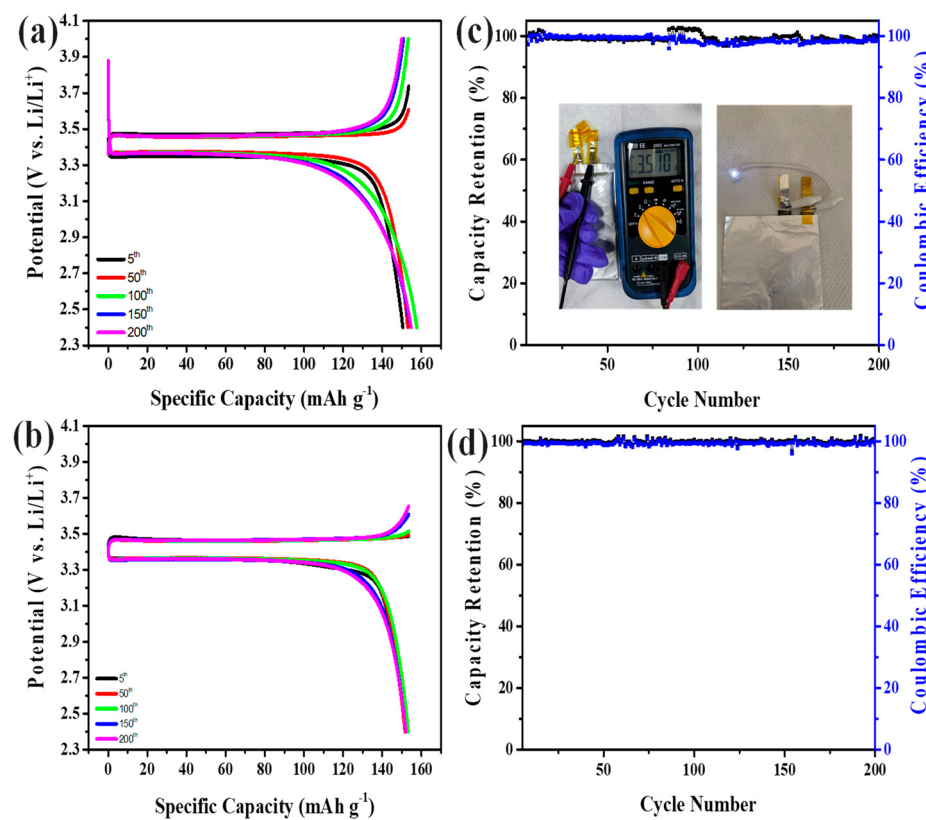


**Figure 7.** Typical charge-discharge curves of different Li-metal batteries using (a) PL31-LATP and (b) PL31-LLZTO electrolytes at 0.2 C (charging) and 0.5 C (discharging). Cyclic performance of different Li-metal batteries using (c) PL31-LATP and (d) PL31-LLZTO electrolytes at 0.2 C (charging) and 0.5 C (discharging). The inset shows the photographs of Li-metal batteries using PL31-LATP electrolytes reaching to ca. 3.51 V) and light-emitting diode lighted on by the solid-state battery.

To facilitate the practical applications, a pouch cell was assembled using an LFP-supported dual composite solid electrolyte (PL31-LATP) and a graphite anode, as shown in the inset of Figure 7c. The digital photograph image demonstrates that the pouch cell successfully powers a light-emitting diode. The pouch cell configuration, comprising LFP cathodes, graphite anodes, and composite solid electrolytes with a thickness around 30  $\mu$ m, achieves an energy density of around 116 Wh kg<sup>-1</sup>. Energy density, cyclic stability, and high-rate capacity are all significantly increased thanks to the cathode-supported hierarchical electrolyte architecture. An improved ionic conductivity and lower interfacial

electrolyte/electrode resistance are the results of this ideal design for composite solid electrolytes. This provides a potentially useful approach to improving energy density, cycle stability, and rate capability in real-world battery applications.

#### 4. Conclusions

This research illustrates the efficacy of a strong composite solid electrolyte design for high-performance Li-metal batteries using LFP cathode sheets, soft polymer (PEO), and Li salt (LiTFSI). The designed solid electrolytes showed superior electrochemical stability above 4.25 V vs. Li/Li<sup>+</sup>. The ESR value exhibits a noteworthy reduction compared to gel electrolytes, owing to the resilient architecture of composite solid electrolytes containing LATP and LLZTO fillers. The observed reduction can be ascribed to the mitigation of bulk electrolyte, charge-transfer, and interfacial electrolyte/electrode impedance. Based on the analysis of EIS measurements, the ionic conductivities of PL31-LATP and PL31-LLZTO electrolytes reach high values of  $2.08 \times 10^{-4}$  and  $1.64 \times 10^{-4}$  S cm<sup>-1</sup>, respectively, at ambient temperature. The Li-metal battery equipped with LFP-supported PL31-LATP electrolyte exhibits not only high-rate capability at 5 C (with a capacity retention of 65.2% compared to the original capacity at 0.2 C), but also superior cyclic stability with excellent Coulombic efficiency (>99.5%) in 200 cycles. These results confirm that the fabricated composite solid electrolyte, composed of PEO, ceramics (LATP and LLZTO), and LiTFSI, acts as a protective layer against the growth of Li dendrites during extended cycling tests, leading to enhanced cyclic stability and desirable rate capability. The composite solid electrolytes developed in this study offer a promising solution for the design of high-performance solid-state electrolytes utilizing LATP ceramic particles.

**Supplementary Materials:** The following supporting information can be downloaded at: <https://www.mdpi.com/article/10.3390/batteries9100490/s1>, Table S1: A comparison table of ionic conductivity based on PEO solid-state electrolyte [47–49].

**Author Contributions:** Conceptualization, C.-T.H. and K.-F.C.; methodology, C.-T.H., P.K.P., K.S.K. and K.-F.C.; resources, C.-T.H.; investigation, K.-F.C., C.-T.H. and P.K.P.; data curation, K.-F.C., P.K.P., N.K., P.-C.Y., K.S.K. and C.-T.H.; software: C.-T.H., K.-F.C. and P.K.P.; formal analysis, C.-T.H., P.K.P., P.-C.Y. and K.S.K.; validation, P.K.P., C.-T.H., P.-C.Y. and K.S.K.; writing—original C.-T.H. and P.K.P.; writing—review and editing, P.K.P., C.-T.H., P.-C.Y. and K.S.K.; visualization, K.-F.C., P.K.P., C.-T.H. and N.K.; supervision, C.-T.H.; project administration, C.-T.H.; funding acquisition, C.-T.H. K.-F.C. and P.K.P. contribute equally to this work. All authors have read and agreed to the published version of the manuscript.

**Funding:** This research was funded by National Science of Technology Council (NSTC) Taiwan, through grant number NSTC 112-2221-E-155-005-MY3.

**Data Availability Statement:** Data is contained within the article.

**Acknowledgments:** The authors gratefully acknowledge the financial support of the National Science of Technology Council (NSTC) Taiwan. Additionally, the authors express their appreciation for the equipment support received from Gold Carbon Inc. (Taoyuan, Taiwan).

**Conflicts of Interest:** The authors declare no conflict of interest.

#### References

1. Tarascon, J.M.; Armand, M. Issues and challenges facing rechargeable lithium batteries. *Nature* **2001**, *414*, 359–367. [[CrossRef](#)] [[PubMed](#)]
2. Nitta, N.; Wu, F.; Lee, J.T.; Yushin, G. Li-ion battery materials: Present and future. *Mater. Today* **2015**, *18*, 252–264. [[CrossRef](#)]
3. Janek, J.; Zeier, W.G. A solid future for battery development. *Nat. Energy* **2016**, *1*, 16141. [[CrossRef](#)]
4. Xu, K. Electrolytes and interphases in Li-ion batteries and beyond. *Chem. Rev.* **2014**, *114*, 11503–11618. [[CrossRef](#)] [[PubMed](#)]
5. Chen, C.; Li, Q.; Li, Y.; Cui, Z.; Guo, X.; Li, H. Sustainable interfaces between Si anodes and garnet electrolytes for room-temperature solid-state batteries. *ACS Appl. Mater. Interfaces* **2018**, *10*, 2185–2190. [[CrossRef](#)]
6. Song, S.W.; Lee, K.C.; Park, H.Y. High-performance flexible all-solid-state micro batteries based on solid electrolyte of lithium boron oxynitride. *J. Power Source* **2016**, *328*, 311–317. [[CrossRef](#)]

7. Hammami, A.; Raymond, N.; Armand, M. Lithium-ion batteries: Runaway risk of forming toxic compounds. *Nature* **2003**, *424*, 635–636. [[CrossRef](#)]
8. Wang, D.; Zhong, G.; Li, Y.; Gong, Z.; McDonald, M.J.; Mi, J.-X.; Fu, R.; Shi, Z.; Yang, Y. Enhanced ionic conductivity of  $\text{Li}_{3.5}\text{Si}_{0.5}\text{P}_{0.5}\text{O}_4$  with addition of lithium borate. *Solid State Ion.* **2015**, *283*, 109–114. [[CrossRef](#)]
9. Takada, K. Progress in solid electrolytes toward realizing solid-state lithium batteries. *J. Power Source* **2018**, *394*, 74–85. [[CrossRef](#)]
10. Jiang, B.; Wei, Y.; Wu, J.; Cheng, H.; Yuan, L.; Li, Z.; Xu, H.; Huang, Y. Recent progress of asymmetric solid-state electrolytes for lithium/sodium-metal batteries. *Energy Chem* **2021**, *3*, 100058. [[CrossRef](#)]
11. Chen, S.Y.; Hsieh, C.T.; Zhang, R.S.; Mohanty, D.; Gandomi, Y.A.; Hung, I.M. Hybrid solid state electrolytes blending NASICON-Type  $\text{Li}_{1+x}\text{Al}_x\text{Ti}_{2-x}(\text{PO}_4)_3$  with poly(vinylidene fluoride-co-hexafluoropropene) for lithium metal batteries. *Electrochim. Acta* **2022**, *427*, 140903. [[CrossRef](#)]
12. Wang, S.; Ben, L.; Li, H.; Chen, L. Identifying  $\text{Li}^+$  ion transport properties of aluminum doped lithium titanium phosphate solid electrolyte at wide temperature range. *Solid State Ion.* **2014**, *268 Pt A*, 110–116. [[CrossRef](#)]
13. Zhang, Z.; Zhao, Y.; Chen, S.; Xie, D.; Yao, X.; Cui, P.; Xu, X. An advanced construction strategy of all-solid-state lithium batteries with excellent interfacial compatibility and ultralong cycle life. *J. Mater. Chem. A* **2017**, *5*, 16984–16993. [[CrossRef](#)]
14. Kim, D.H.; Oh, D.Y.; Park, K.H.; Choi, Y.E.; Nam, Y.J.; Lee, H.A.; Lee, S.M.; Jung, Y.S. Infiltration of solution-processable solid electrolytes into conventional Li-ion-battery electrodes for all-solid-state Li-ion batteries. *Nano Lett.* **2017**, *17*, 3013–3020. [[CrossRef](#)]
15. Koerver, R.; Aygün, I.; Leichtweiß, T.; Dietrich, C.; Zhang, W.; Binder, J.O.; Hartmann, P.; Zeier, W.G.; Janek, J. Capacity fade in solid-state batteries: Interphase formation and chemomechanical processes in nickel-rich layered oxide cathodes and lithium thiophosphate solid electrolytes. *Chem. Mater.* **2017**, *29*, 5574–5582. [[CrossRef](#)]
16. Zhang, B.; Tan, R.; Yang, L.; Zheng, J.; Zhang, K.; Mo, S.; Lin, Z.; Pan, F. Mechanisms and properties of ion-transport in inorganic solid electrolytes. *Energy Storage Mater.* **2018**, *10*, 139–159. [[CrossRef](#)]
17. Zhou, Q.; Ma, J.; Dong, S.; Li, X.; Cui, G. Intermolecular chemistry in solid polymer electrolytes for high-energy-density lithium batteries. *Adv. Mater.* **2019**, *31*, 190209. [[CrossRef](#)]
18. Yan, Y.; Ju, J.; Dong, S.; Wang, Y.; Huang, L.; Cui, L.; Jiang, F.; Wang, Q.; Zhang, Y.; Cui, G. In situ polymerization permeated three-dimensional  $\text{Li}^+$ -percolated porous oxide ceramic framework boosting All solid-state lithium metal battery. *Adv. Sci.* **2021**, *8*, 2003887. [[CrossRef](#)]
19. Lv, Z.; Zhou, Q.; Zhang, S.; Dong, S.; Wang, Q.; Huang, L.; Chen, K.; Cui, G. Cyano-reinforced in-situ polymer electrolyte enabling long-life cycling for high-voltage lithium metal batteries. *Energy Storage Mater.* **2021**, *37*, 215–223. [[CrossRef](#)]
20. Cui, G. Reasonable design of high-energy-density solidstate lithium-metal batteries. *Matter* **2020**, *2*, 805–815. [[CrossRef](#)]
21. Nie, K.; Wang, X.; Qiu, J.; Wang, Y.; Yang, Q.; Xu, J.; Yu, X.; Li, H.; Huang, X.; Chen, L. Increasing poly(ethylene oxide) stability to 4.5 V by surface coating of the cathode. *ACS Energy Lett.* **2020**, *5*, 826–832. [[CrossRef](#)]
22. Zhang, J.; Zhao, N.; Zhang, M.; Li, Y.; Chu, P.K.; Guo, X.; Di, Z.; Wang, X.; Li, H. Flexible and ion-conducting membrane electrolytes for solid-state lithium batteries: Dispersion of garnet nanoparticles in insulating polyethylene oxide. *Nano Energy* **2016**, *28*, 447–454. [[CrossRef](#)]
23. Wang, L.P.; Zhang, X.D.; Wang, T.S.; Yin, Y.X.; Shi, J.L.; Wang, C.R.; Guo, Y.G. Ameliorating the interfacial problems of cathode and solid-state electrolytes by interface modification of functional polymers. *Adv. Energy Mater.* **2018**, *8*, 1801528. [[CrossRef](#)]
24. Sung, P.Y.; Lu, M.; Hsieh, C.T.; Gandomi, Y.A.; Gu, S.; Liu, W.R. Sodium super ionic conductor-type hybrid electrolytes for high performance lithium metal batteries. *Membranes* **2023**, *13*, 201. [[CrossRef](#)] [[PubMed](#)]
25. Wang, M.; Xue, Y.; Zhang, K.; Zhang, Y. Synthesis of  $\text{FePO}_4 \cdot 2\text{H}_2\text{O}$  nanoplates and their usage for fabricating superior high-rate performance  $\text{LiFePO}_4$ . *Electrochim. Acta* **2011**, *56*, 4294–4298. [[CrossRef](#)]
26. Hsieh, C.T.; Pai, C.T.; Chen, Y.F.; Chen, I.L.; Chen, W.Y. Preparation of lithium iron phosphate cathode materials with different carbon contents using glucose additive for Li-ion batteries. *J. Taiwan Inst. Chem. Eng.* **2014**, *45*, 1501–1508. [[CrossRef](#)]
27. Polu, A.R.; Kumar, R.; Rhe, H.W. Magnesium ion conducting solid polymer blend electrolyte based on biodegradable polymers and application in solid-state batteries. *Ionics* **2015**, *21*, 125–132. [[CrossRef](#)]
28. Marceau, H.; Kim, C.S.; Paoella, A.; Ladouceur, S.; Lagacé, M.; Chaker, M.; Vijh, A.; Guerfi, A.; Julien, C.M.; Mauger, A.; et al. In operando scanning electron microscopy and ultraviolet-visible spectroscopy studies of lithium/sulfur cells using all solid-state polymer electrolyte. *J. Power Source* **2016**, *319*, 247–254. [[CrossRef](#)]
29. Liang, Y.; Lin, Z.; Qiu, Y.; Zhang, X. Fabrication and characterization of LATP/PAN composite fiber-based lithium-ion battery separators. *Electrochim. Acta* **2011**, *56*, 6474–6480. [[CrossRef](#)]
30. Kumar, J.; Kichambare, P.; Rai, A.K.; Bhattacharya, R.; Rodrigues, S.; Subramanyam, G.A. A high performance ceramic-polymer separator for lithium batteries. *J. Power Source* **2016**, *301*, 194–198. [[CrossRef](#)]
31. Yoon, S.A.; Oh, N.R.; Yoo, A.R.; Lee, H.G.; Lee, H.C. Preparation and characterization of Ta-substituted  $\text{Li}_7\text{La}_3\text{Zr}_{2-x}\text{O}_{12}$  garnet solid electrolyte by sol-gel processing. *J. Korean Ceram. Soc.* **2017**, *54*, 278–284. [[CrossRef](#)]
32. Xie, H.; Li, C.; Kan, W.H.; Avdeev, M.; Zhu, C.; Zhao, Z.; Chu, X.; Mu, D.; Wu, F. Consolidating the grain boundary of the garnet electrolyte LLZTO with  $\text{Li}_3\text{BO}_3$  for high-performance  $\text{LiNi}_{0.8}\text{Co}_{0.1}\text{Mn}_{0.1}\text{O}_2/\text{LiFePO}_4$  hybrid solid batteries. *J. Mater. Chem. A* **2019**, *7*, 20633–20639. [[CrossRef](#)]
33. Prasanna, K.; Subburaj, T.; Lee, W.J.; Lee, C.W. Polyethylene separator: Stretched and coated with porous nickel oxide nanoparticles for enhancement of its efficiency in Li-ion batteries. *Electrochim. Acta* **2014**, *137*, 273–279. [[CrossRef](#)]

34. Fan, X.; Chen, L.; Ji, X.; Deng, T.; Hou, S.; Chen, J.; Zheng, J.; Wang, F.; Jiang, J.; Xu, K.; et al. Highly fluorinated interphases enable high-voltage Li-metal batteries. *Chem.* **2018**, *4*, 174–185. [[CrossRef](#)]
35. Girard, G.M.A.; Hilder, M.; Nucciarone, D.; Whitbread, K.; Zavorine, S.; Moser, M.; Forsyth, M.; MacFarlane, D.R.; Howlett, P.C. Role of Li concentration and the SEI layer in enabling high performance Li metal electrodes using a phosphonium bis(fluorosulfonyl)imide ionic liquid. *J. Phys. Chem. C* **2017**, *121*, 21087–21095. [[CrossRef](#)]
36. Hsieh, C.T.; Pai, C.T.; Chen, Y.F.; Yu, P.Y.; Juang, R.S. Electrochemical performance of lithium iron phosphate cathodes at various temperatures. *Electrochim. Acta* **2014**, *115*, 96–102. [[CrossRef](#)]
37. Samsinger, R.F.; Schopf, S.O.; Schuhmacher, J.; Treis, P.; Schneider, M.; Roters, A.; Kwade, A. Influence of the processing on the ionic conductivity of solid-state hybrid electrolytes based on glass-ceramic particles dispersed in PEO with LiTFSI. *J. Electrochem. Soc.* **2020**, *167*, 120538. [[CrossRef](#)]
38. Panda, A.; Patra, J.P.; Hsieh, C.T.; Huang, Y.C.; Gandomi, Y.A.; Fu, C.C.; Lin, M.H.; Juang, R.S.; Chang, J.K. Improving high-temperature performance of lithium-rich cathode by roll-to-roll atomic layer deposition of titania nanocoating for lithium-ion batteries. *J. Energy Storage* **2021**, *44*, 103348. [[CrossRef](#)]
39. Nien, Y.H.; Carey, J.R.; Chen, J.S. Physical and electrochemical properties of LiFePO<sub>4</sub>/C composite cathode prepared from various polymer-containing precursors. *J. Power Source* **2009**, *193*, 822–827. [[CrossRef](#)]
40. Wu, H.C.; Wu, H.C.; Lee, E.; Wu, N.L. High-temperature carbon-coated aluminum current collector for enhanced power performance of LiFePO<sub>4</sub> electrode of Li-ion batteries. *Electrochim. Commun.* **2010**, *12*, 488–491. [[CrossRef](#)]
41. Wang, W.; Yi, E.; Fici, A.J.; Laine, R.M.; Kieffer, J. Lithium ion conducting poly(ethylene oxide)-based solid electrolytes containing active or passive ceramic nanoparticles. *J. Phys. Chem. C* **2017**, *121*, 2563–2573. [[CrossRef](#)]
42. Xu, G.; Li, F.; Tao, Z.; Wei, X.; Liu, Y.; Li, X.; Ren, Z.; Shen, G.; Han, G. Monodispersed LiFePO<sub>4</sub>@C core–shell nanostructures for a high power Li-ion battery cathode. *J. Power Source* **2014**, *246*, 696–702. [[CrossRef](#)]
43. Yu, S.; Schmidt, R.D.; Garcia-Mendez, R.; Herbert, E.; Dudney, N.J.; Wolfenstine, J.B.; Sakamoto, J.; Siegel, D.J. Elastic properties of the solid electrolyte Li<sub>7</sub>La<sub>3</sub>Zr<sub>2</sub>O<sub>12</sub> (LLZO). *Chem. Mater.* **2015**, *28*, 197–206. [[CrossRef](#)]
44. Yan, G.; Malzbender, J.; Fu, S.; Gross, J.P.; Yu, S.; Eichel, R.-A.; Schwaiger, R. Fracture behavior of solid electrolyte LATP material based on micro-pillar splitting method. *J. Eur. Ceram. Soc.* **2021**, *41*, 5240–5247. [[CrossRef](#)]
45. Huo, H.; Chen, Y.; Luo, J.; Yang, X.; Guo, X.; Sun, X. Rational design of hierarchical “ceramic-in-polymer” and “polymer-in-ceramic” electrolytes for dendrite-free solid-state batteries. *Adv. Energy Mater.* **2019**, *9*, 1804004. [[CrossRef](#)]
46. Tornheim, A.; O’Hanlon, D.C. What do coulombic efficiency and capacity retention truly measure? A deep dive into cyclable lithium inventory, limitation type, and redox side reactions. *J. Electrochem. Soc.* **2020**, *167*, 110520. [[CrossRef](#)]
47. Zhao, Y.; Huang, Z.; Chen, S.; Chen, B.; Yang, J.; Zhang, Q.; Ding, F.; Chen, Y.; Xu, X. A promising PEO/LAGP hybrid electrolyte prepared by a simple method for all-solid-state lithium batteries. *Solid State Ionics* **2016**, *295*, 65–71. [[CrossRef](#)]
48. Wan, Z.; Lei, D.; Yang, W.; Liu, C.; Shi, K.; Hao, X.; Shen, L.; Lv, W.; Li, B.; Yang, Q.-H.; et al. Low resistance–integrated all-solid-state battery achieved by Li<sub>7</sub>La<sub>3</sub>Zr<sub>2</sub>O<sub>12</sub> nanowire upgrading polyethylene oxide (PEO) composite electrolyte and PEO cathode binder. *Adv. Funct. Mater.* **2019**, *29*, 1–10. [[CrossRef](#)]
49. Zhu, L.; Zhu, P.H.; Fang, Q.X.; Jing, M.X.; Shen, X.Q.; Yang, L.Z. A novel solid PEO/LLTO-nanowires polymer composite electrolyte for solid-state lithium-ion battery. *Electrochim. Acta* **2018**, *292*, 718–726. [[CrossRef](#)]

**Disclaimer/Publisher’s Note:** The statements, opinions and data contained in all publications are solely those of the individual author(s) and contributor(s) and not of MDPI and/or the editor(s). MDPI and/or the editor(s) disclaim responsibility for any injury to people or property resulting from any ideas, methods, instructions or products referred to in the content.